PAPER • **OPEN ACCESS**

A novel plasma source concept for negative ion generation in neutral beam injectors for fusion applications

To cite this article: G Chitarin *et al* 2024 *Plasma Phys. Control. Fusion* **66** 115018

OPEN ACCESS
IOP Publishing
Plasma Physics and Controlled Fusion
Plasma Phys. Control. Fusion **66** (2024) 115018 (9pp)
https://doi.org/10.1088/1361-6587/ad814d

A novel plasma source concept for negative ion generation in neutral beam injectors for fusion applications

G Chitarin[1,2], D Abate[2], F Elio[3], E Sartori[1,2] and G Spizzo[2,4,*]

[1] University of Padova, DTG, Department of Management and Engineering, Strad. S. Nicola 3, 36100 Vicenza, Italy
[2] Consorzio RFX (CNR, ENEA, INFN, Università di Padova, Acciaierie Venete SpA), Corso Stati Uniti 4, 35127 Padova, Italy
[3] Deutelio, Via Calcinate 31, 21026 Gavirate, Italy
[4] Istituto per la Scienza e la Tecnologia dei Plasmi del CNR, Corso Stati Uniti 4, 35127 Padova, Italy

E-mail: gianluca.spizzo@igi.cnr.it and giuseppe.chitarin@unipd.it

Received 17 May 2024, revised 20 September 2024
Accepted for publication 26 September 2024
Published 11 October 2024

Abstract

A low-temperature plasma can very well be confined by a simple magnetic dipole, such as in the Van Allen belts of Earth's magnetosphere. This configuration can be reproduced in laboratory as a small experimental device, designed in such a way that the magnetic field lines remain within a vacuum-tight container and are virtually not intercepted by the container wall. In this paper we propose to use a dipole field for the realization of an efficient negative Ion source. To this purpose, we analyze the plasma confinement capabilities of such plasma source, in order to assess the equilibrium pressure and estimate the particle trajectories and drifts.

Keywords: plasma sources, particle beams, magnetic confinement, magnetic mirrors and cusps, low-temperature plasmas

1. Introduction

Negative ion sources used for fusion applications are required to produce up to ∼50 A of Hydrogen or Deuterium ion current from a low-temperature (few eV) plasma. Considering that the negative ion current is typically in the range ∼200–300 A m^{-2} at the extraction apertures (where gas pressure is kept <0.3 Pa, to avoid excessive neutral gas flow in the accelerator), these sources can be quite large and their input power ranges from some tens to hundreds of kW [1].

Two types of Negative Ion Sources are currently used for fusion experiments: the first is the Japanese filament-arc sources, where hot biased filaments produce an arc plasma discharge, which is confined inside a 'plasma box' by a multicusp magnetic configuration. An example is the 'kamaboko' source described in [2], and it is generated by permanent magnets. The configuration is sketched in figure 1(a). The second one is the class of RF (radio-frequency) plasma-driver sources, mainly developed in Europe, where a coil operating at about 1–2 MHz induces a plasma discharge inside a cylindrical volume surrounded by thick metallic shields [3]. In this second case, the confining magnetic field is *outside* the metallic box, as shown in figure 1(b).

The generated plasma expands towards a cesiated Plasma Grid (PG), where some of the impinging particles are converted into negative ions and then accelerated through the grid apertures. In both source types, a power of about 1–4 MW m^{-2} is necessary for achieving the required negative ion current

* Author to whom any correspondence should be addressed.

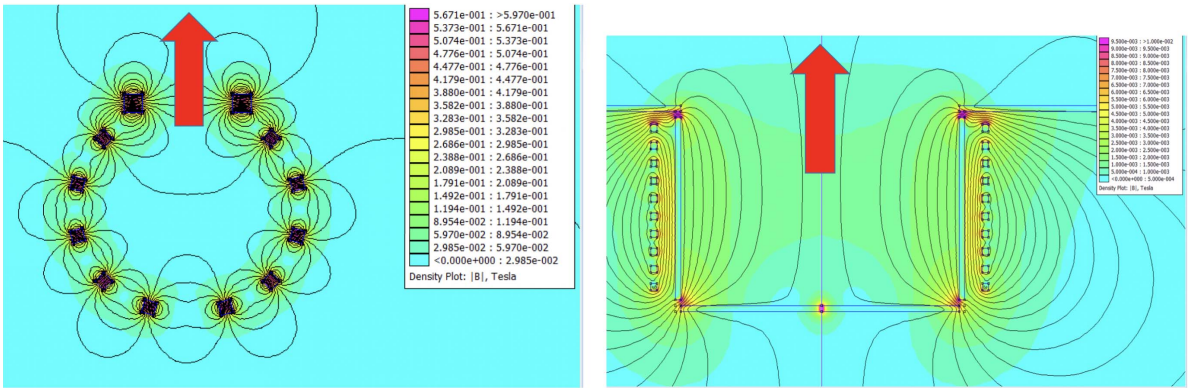

(a) (b)

Figure 1. (a) Kamaboko plasma source, which is a planar multi-cusp, magnetic DC configuration; (b) the cylindrical RF-driver plasma source, which is an axially symmetric magnetic configuration. The red arrows indicate the direction of ion extraction.

to be extracted at the grid. This reveals the limitations of the existing negative ion sources, which, depending on the adopted technology, are:

- for RF sources, magnetic field lines intercepting the plasma chamber determine fast parallel transport of particles to the wall;
- a large fraction of the electric power of the RF coils is also dissipated by eddy currents induced on the metallic structures of the RF driver [4];
- for kamaboko sources, regular access is required for maintenance, due to the limited lifetime of the Tungsten filaments [5];
- for both source types, strong particle drifts and non-uniformity of the extracted beam is typically caused by the transverse magnetic field, which is necessary for filtering out the $E \gtrsim 1$ eV electrons, that have a high probability of destroying negative ions by impact in the extraction region.

The efficiency of the negative ion source has a considerable impact on the fusion power gain, defined as $Q = P_{\text{fusion}}/P_{\text{heating}}$, of any fusion device based on magnetic confinement and neutral beam injectors heating [6]. For these reasons, in this paper we propose and describe the project of a negative ion source based on a simple dipole configuration [7]. The scheme has in principle various advantages: the dipole magnetic configuration is well-known since the 70's in geophysics [8] and it is a rather simple geometry to be realized in laboratory; it is characterized by an intrinsic high beta, and, last but not least, the magnetic field is placed *inside* the ion source, thus avoiding the dissipation of RF power which plagues present-day ion source schemes [3]. Therefore, in principle a dipole ion source has a higher efficiency with respect to the ion sources available nowadays. The paper is organized as follows: section 2 discusses the overall magnetohydrodynamic equilibrium of the dipole source, section 3 shows an initial estimate of particle trajectories and expected neoclassical effects, while in section 4 we draw our conclusions.

2. Plasma confinement in a purely poloidal magnetic field

Plasma sources, contrary to magnetic confinement devices as, for example, the tokamak, are current-free plasmas. Therefore, the low-temperature plasma in the source can be confined using a configuration with a purely poloidal magnetic field. Such a configuration has the clear advantage that the magnetic field lines do not cross the solid walls of the device and thus most of the electron trajectories are not intercepted by a material wall. Among the configurations with poloidal magnetic field only, the dipole can achieve plasma pressure equilibrium with no induced plasma current. Moreover, the dipole configuration is also intrinsically stable with respect to ideal magnetohydrodynamic (MHD) $m = 1$ and $m = 0$ modes (or at least, at very high beta values, $\beta < 86\%$, β being the ratio between kinetic and magnetic pressure, see equation (1) and [9]). In fact, the dipole with B_θ field, only, can be considered as a toroidal version of the 'hard-core Z-pinch' [9]. The concept of plasma confinement in a dipole configuration is not new: it has already been applied for nuclear fusion experiments, following the pioneering work of Hasegawa [10], in the Levitating Dipole eXperiment (LDX) which was operated in years 2004–2011 at the Columbia University [11]. LDX obtained record values of $\beta \approx 25\%$, much larger than in the tokamak [12]. A dipole configuration has also been proposed in the Polomac device [13], which does not require the levitation of a superconducting coil, that is the main ingredient of the Hasegawa scheme, but goes back to the older design of a supported ring devised in the 60's by Bo Lehnert [14, 15]. Finally, a small device for magnetron sputtering has been realized using the dipole configuration produced via permanent magnets [16].

In this paper we propose a new plasma driver based on the dipole configuration: the device is shown in figure 2. It consists

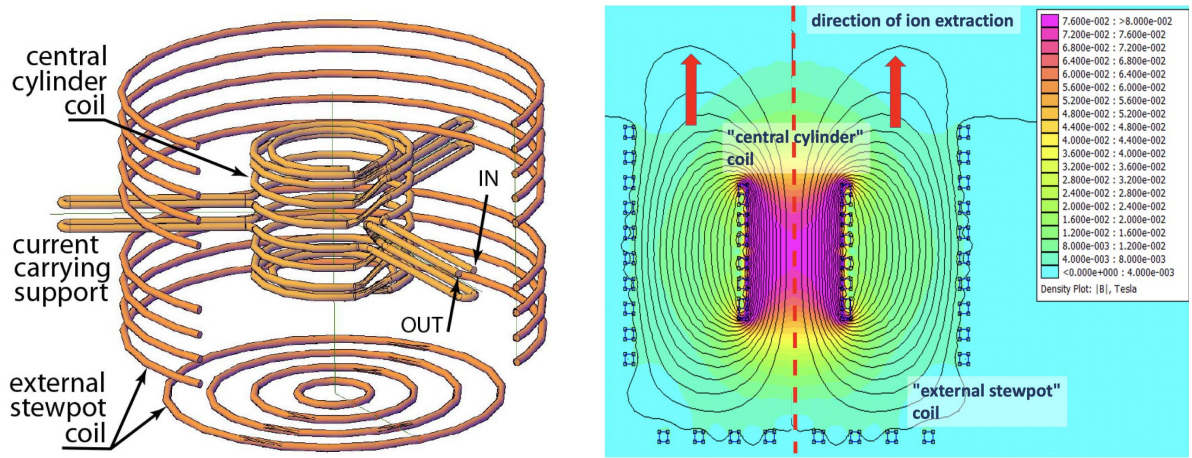

(a) (b)

Figure 2. (a) CAD view of the coil system of the proposed plasma driver; and (b) the corresponding magnetic field configuration. The system has axial symmetry along $\hat{z}$.

in a *central cylinder* coil, placed inside a larger *external stewpot* coil, as shown in figure 2(a). The device will be contained in a vacuum vessel and has axial symmetry along the coordinate $\hat{z}$, similarly to the RF driven plasma sources [3], but with smaller size: it is a scaled-down, proof-of-principle prototype for the ITER NBI ion source. The radii of the two coils are $r_c = 40$ mm and $r_p = 120$ mm, respectively; the overall diameter of the device is about 250 mm (including the necessary space for the coil feeder) and about 200 mm in height. The radius r_p of the 'stewpot' coil can be considered as the maximum plasma radius. The central coil produces a steady-state poloidal magnetic field $B_\theta(r)$ of maximum amplitude ≈ 80 mT, which is large inside the cylinder and decreases rapidly outside, as shown in figure 2(b). The field decays like $\sim 1/r$ for $r > r_c$, as shown in figure 5(b).

The rapid decay of the magnetic field with radius stabilizes the plasma $m = 1$ ideal mode, which is the major problem of the Z-pinch [9]. Plasma pressure vanishes just outside the central cylinder coil, then peaks and decreases again for large r, and it is mainly due to a diamagnetic effect which guarantees the MHD equilibrium of the configuration, as we will discuss more in detail in section 2.2. A similar mechanism governs the Van Allen belts [8] and was observed on LDX, too [17]. Figure 2(a) shows a CAD view of the dipole plasma driver: the central cylinder coil is constituted by water-cooled current-carrying conductors; the external stewpot coil is also constituted by water-cooled conductors, while three current-carrying supports also provide magnetic shielding to reduce heat load on the supports themselves.

Three options are considered possible for producing a plasma inside the 'stewpot' coil, namely:

(i) filament-driven arc discharge, using a hot Tungsten filament (heated by a DC current) and negatively polarized with respect to the vacuum vessel (and the coils) with a voltage of 10–30 Volt DC, so as to produce a steady-state arc discharge.

(ii) radio-frequency (RF) heating, by superimposing a relatively small sinusoidal current (with a frequency of the order of the ion cyclotron frequency $\approx$ 0.1–2.0 MHz) to the much larger DC current in the central cylinder coil.

(iii) microwave heating, using an external microwave source (magnetron, with a frequency of the order of the electron cyclotron frequency $\approx$0.2–2.45 GHz) with a truncated waveguide or a horn antenna and a vacuum-tight window.

In all cases, access for heating is possible on the lower external part of the stewpot coil (see figure 2(b)). We will probably use a simple filament-driven arc discharge for the first plasma experiments.

2.1. Estimate of beta

A first estimate of the plasma beta in our device can be obtained from global pressure balance in a Z-pinch equilibrium. Following Freidberg [9], we define beta as

$$\beta = \frac{16\pi^2}{\mu_0 (I_c + I_p)^2} \int_{r_c}^{\infty} p(r)\, r\, dr\,, \tag{1}$$

where $p(r)$ is the radial profile of the plasma pressure, I_c is the current flowing in the coils and I_p is the plasma current. Equation (1) can be easily understood considering that the magnetic field far from the plasma approaches $\mu_0(I_c + I_p)/2\pi$. Starting from the equation of the radial pressure balance for the general screw pinch [18] (with $B_\phi = 0$), a simple calculation shows that β, defined as in equation (1), can be related with the current in the coils through

$$\beta = 1 - \left(\frac{1}{1 + I_p/I_c}\right)^2 . \tag{2}$$

In our system, the central coil current is $I_c = 1$ kA $\times$ 8 turns $= 8$ kA, while we can assume the plasma diamagnetic current to be less than 1% of the central coil current [19], namely I_p

$\sim$ 80 A. In this way, according to equation (2), it should be $\beta \approx 2\%$. This is anyway a lower bound for the plasma beta. In fact, in a dipole the magnetic field can be much larger in the central area of the cylinder (purple color in figure 2(b)): in fact, a dipole can be seen as the limit for $r \to 0$ of a loop with current I and radius r, keeping the magnetic moment μ = constant. It follows that the current scales as $I = \mu/r^2$, and $I_p/I_c = (r_c/r_p)^2$. Equation (2) then becomes

$$\beta = 1 - \left(\frac{1}{1 + (r_c/r_p)^2} \right)^2 . \tag{3}$$

By inserting the geometry of our device ($r_c = 40$ mm and $r_p = 120$ mm) the beta of a pure dipole would be $\beta = 19\%$. This would correspond to a plasma diamagnetic current of ≈ 890 A, which can be taken as an upper bound for the plasma current. We might therefore expect an operating space of the proposed ion source configuration with values of beta in the interval $\beta \approx 2\%$–19% and corresponding diamagnetic plasma current $I_p \approx 80$–890 A.

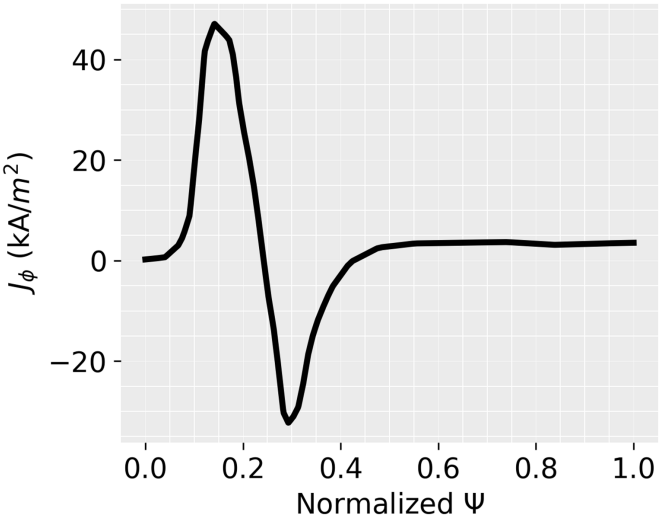

Figure 3. Assumed diamagnetic current density profile $j(\Psi)$, plotted as a function of the normalized poloidal flux Ψ. The parametrization is the same used for the LDX equilibrium ('trifurcated' profile) [20, 22].

2.2. *Force-balance equilibrium*

The force balance axisymmetric equilibrium for a dipole configuration is described through a 2D elliptic partial differential equation [20]:

$$\Delta^* \Psi = \mu_0 \vec{j}, \tag{4}$$

where $\Delta^* = \nabla \cdot \frac{1}{r} \nabla$ is the elliptic operator, Ψ is the poloidal magnetic flux and $\vec{j}$ is the plasma current density. Since there is no toroidal magnetic field, the plasma current is purely diamagnetic, and it is related to the pressure gradient, only, through

$$\vec{j} = -\frac{\nabla p \times \vec{B}}{B^2}. \tag{5}$$

Since the pressure gradient is radial and the field is purely poloidal, it follows from equation (5) that the diamagnetic current is purely toroidal, as observed indeed in LDX [20]. Thus, a purely poloidal vacuum field gives rise to a purely toroidal diamagnetic current, which in turn adds to the poloidal field. Equation (4) is iteratively solved by using the IET code [21] by properly imposing the poloidal magnetic flux at the boundaries of the computational domain (i.e. the central coil and the plasma boundary). The problem in (4) has been solved for two different cases identified by properly defining the right hand side of (4):

(i) Vacuum case, where no plasma current exists (i.e. $\vec{j} = 0$), as shown in figure 2(b);
(ii) Plasma case, where a plasma diamagnetic current density profile has been assumed, shown in figure 4(b).

In the second case, the toroidal current density is assumed to follow the 'trifurcated model' used for equilibrium reconstruction in LDX [20, 22], with a linear transition between the negative toroidal current density inside the pressure peak to the positive toroidal current density outside the peak corresponding to a parabolic pressure profile (see figure 3). Moreover, the boundary conditions at $r = r_p$ and $r = r_c$ are updated iteratively with the contribution of the plasma diamagnetic current.

The solution of problem (ii) is shown in terms of poloidal flux surfaces in figure 4(a) while the related plasma diamagnetic current density is represented in figure 4(b). Note that, while the direction of the current density must change sign in the plasma, there is always a net plasma current that flows in the same direction as the central coil current in order to provide radial force balance [19]. This current is estimated to be less than 1% of the total central cylinder coil current, as anticipated in section 2.1.

The magnitude of the equilibrium poloidal magnetic field is shown in figure 5(a) together with the poloidal magnetic field vector (red arrows). The radial profile of the poloidal magnetic field on the equatorial plane is reported in figure 5(b): the presence of the central cylinder coil leads to a B_θ profile that is large at the surface of the coil and then decreases approximately proportional to $B_\theta \sim 1/r$, although with a superposed diamagnetic depression due to pressure effects [9]. This decay is weaker than the ideal dipole, as we will see in section 3. To better approximate the dipole, we have modified our plasma driver in order to increase the flux in the cylinder by widening the space between r_c and r_p, at the same time decreasing the current in the stewpot coils. The ideal dipole is obtained in fact in the limit $r_c \to 0$, $I_c \to \infty$ and $r_p \to \infty$, see the discussion on equation (3) above.

The effect of the diamagnetic current on the equilibrium can be quantified by comparing the vacuum solution (i) with the plasma solution (ii): since the impact of diamagnetic current is relatively low both in terms on poloidal flux (figure 6(a)) and poloidal magnetic field (figure 6(b)), we can assume

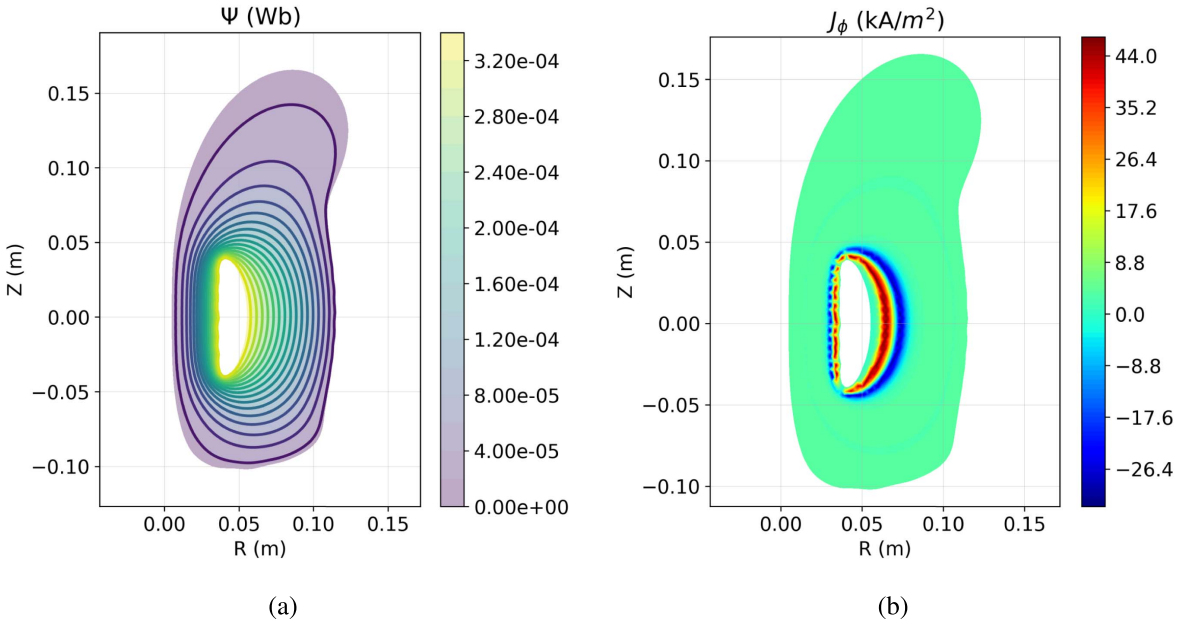

Figure 4. Equilibrium configuration obtained by solving (4) with the trifurcated current profile of figure 3 in terms of poloidal flux surfaces (a) and plasma diamagnetic current density (b). The presence of the toroidal diamagnetic current provides plasma equilibrium.

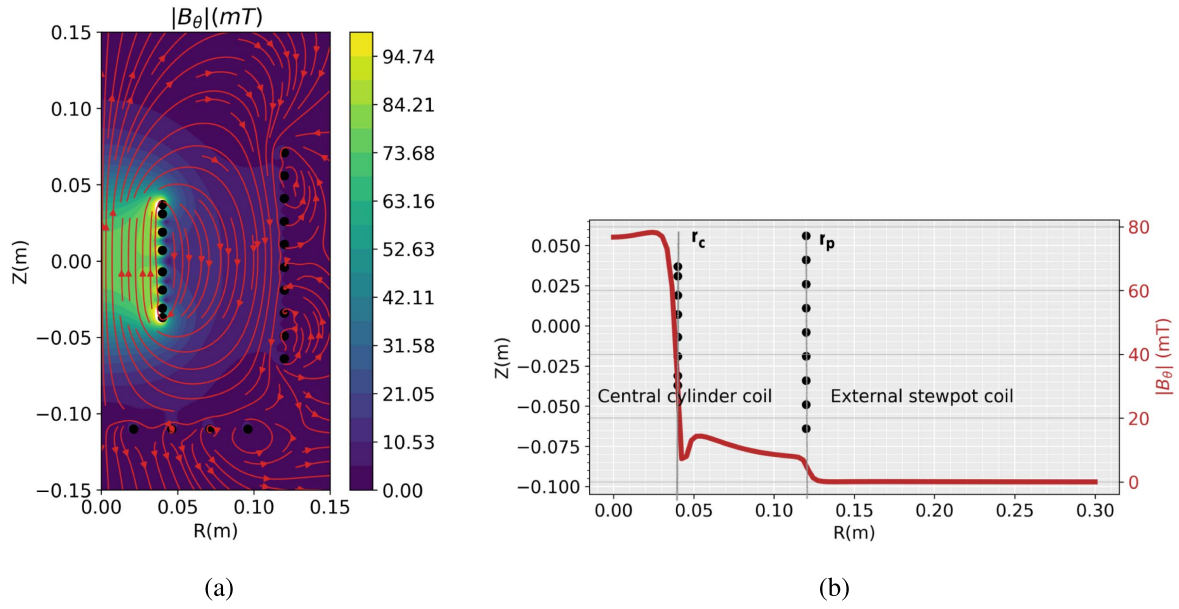

Figure 5. (a) Contour plot of magnetic field magnitude $|B|$ with overplotted $\vec{B}$ vector map (red arrows); (b) radial profile of poloidal magnetic field $B_\theta(r)$ on the equatorial plane.

that the equilibrium magnetic field with plasma can be well approximated by the vacuum solution. This result is consistent with the assumed ratio $I_p/I_c \approx 1\%$, as discussed above and in section 2.1.

3. Particle trajectories and neoclassical transport

The rather simple dipole geometry, which has been seen in solving equation (4), leads to simpler particle orbits than in tokamak and stellarator configurations. In fact, the ideal (or point) dipole is represented in spherical coordinates (r,θ,ϕ), where (r,ϕ) are similar to toroidal coordinates, while the elevation $\theta = 0$ on the upper pole, and $\theta = \pi/2$ on the equatorial plane. The resulting analytic expression [23] is:

$$\vec{B} = \frac{\sin\theta\,\hat{\theta} + 2\cos\theta\,\hat{r}}{r^3}\,, \tag{6}$$

with corresponding magnitude:

$$B = \frac{\sqrt{3\cos^2\theta + 1}}{r^3}\,. \tag{7}$$

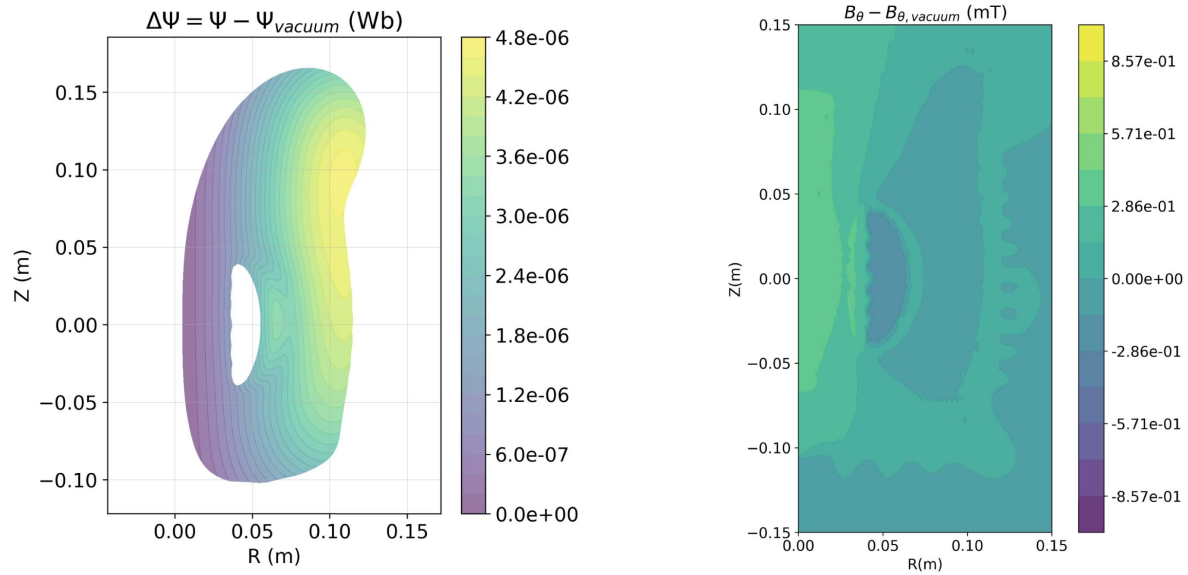

Figure 6. Impact of diamagnetic current in terms of poloidal magnetic flux (a) and magnitude of the poloidal magnetic field (b).

In the dipole approximation, the poloidal flux is $\Psi = \sin^2\theta/r$ and the resulting field strength is $B \sim 1/r^3$, which is a stronger decay than what predicted in our device, see figure 5(b). Despite this, the point dipole is a good approximation of particle orbits in our device. The poloidal flux decays like $\Psi \sim 1/r$, which is consistent with equations (4) and (5). From the point of view of particle motion, the absence of toroidal field implies the absence of drifts across the poloidal flux surfaces, $\dot{\Psi} = 0$. Trapped particles follow closed orbits on the poloidal plane, corresponding to zero-width bananas: therefore, a dipole is characterized by negligible neoclassical transport, contrary to tokamaks and stellarators. Toroidal precession, which is proportional to $\dot{\phi} \approx B_\theta \dfrac{\partial B}{\partial \Psi}$, is instead rather strong, due to the presence of the radial derivative of the field magnitude [24]. Contrary to tokamaks, passing particles also possess closed orbits lying on the poloidal plane, and precede along the toroidal angle ϕ, in all respects similar to banana orbits. Trapped particles are anyway the majority in a dipole configuration. An initial estimate of the trapped fraction in our device can be done by using the traditional expression [25]:

$$\lambda(\Psi,\theta) = \sqrt{1 - \frac{B(\Psi,\theta)}{B(\Psi,\theta_b)}}\,, \tag{8}$$

where $\lambda = v_\parallel/v$ is the ratio between parallel and total velocity, a.k.a. particle 'pitch', and θ_b is the 'bounce angle', namely the angle where the particle bounces back on the magnetic mirror. As anticipated above, particles can either be trapped, following closed 'banana orbits' outside the central cylinder coil (figure 8(a)), or can enter inside the central cylinder coil, circulating on the poloidal angle (figure 8(b)). The critical condition is when the bounce angle touches the axis of the device, namely $\theta_b = 0$. Note that equation (8) is expressed in spherical coordinates, therefore $\theta = 0$ corresponds to the axis of the central cylinder coil ($z = 0$, $r < r_c$) and $\theta = \pi/2$ corresponds to the outer equatorial plane ($z = 0$, $r > r_c$). Inserting $\theta_b = 0$ in equation (8) one can write the critical pitch as

$$\lambda_c(\Psi,\theta) = \sqrt{1 - \frac{B(\Psi,\theta)}{B(\Psi,0)}}\,. \tag{9}$$

Particles whose pitch is smaller than the critical $\lambda < \lambda_c$ are trapped, while passing particles have $\lambda \geqslant \lambda_c$. The map of λ_c, for the equilibrium fields calculated in section 2.2, is shown in figure 7(a): in large part of the plasma volume, for radii in between $r_c < r < r_p$, the critical pitch $\lambda_c \approx 0.9$. This means that 90% of particles are trapped and they perform banana trajectories along the field lines shown in figure 5(a). This phenomenon is well known in Earth's magnetosphere, where the majority of ions are trapped in the Van Allen belts [8], and it is the reason for the very good particle confinement which was measured in the LDX device [12].

The bounce angles θ_b of the banana trajectories can be evaluated analytically for the point dipole equilibrium: using again equation (8) and considering particles deposited on the outer midplane at $\theta = \pi/2$ with a given pitch $0 < \lambda < 1$, we can express the equation in terms of θ_b, thus obtaining:

$$B(r,\theta_b) = \frac{B\left(r,\dfrac{\pi}{2}\right)}{1-\lambda^2}\,. \tag{10}$$

Now insert equation (7) in (10), taking care that orbits conserve the poloidal flux Ψ, therefore one must substitute

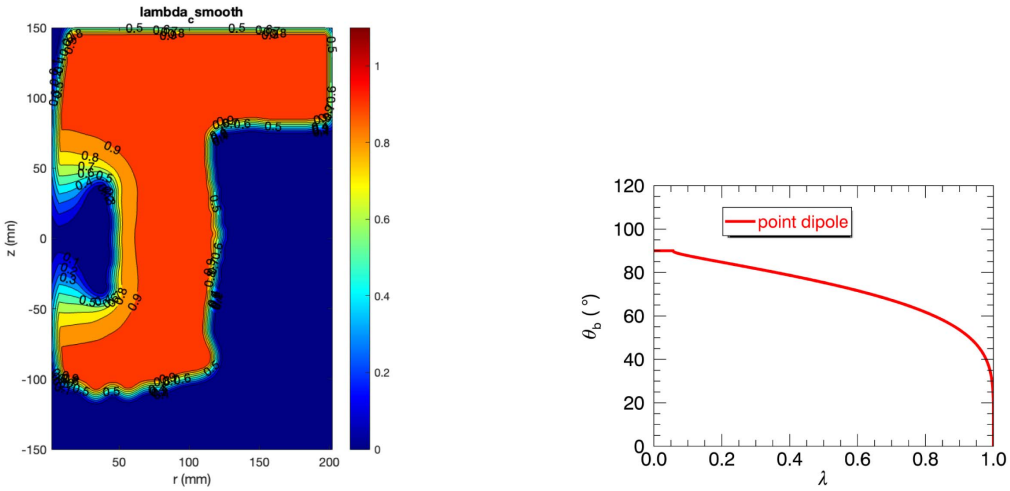

(a) (b)

Figure 7. (a) Map of critical pitch, for the realistic fields of the plasma source calculated in section 2.2; (b) bounce angle θ_b as a function of pitch, ideal dipole field of equation (6).

$r = \sin^2\theta/\Psi$. In this way, we end up with an implicit equation for the bounce angle:

$$\frac{\sqrt{3\cos^2\theta_b + 1}}{\sin^6\theta_b} = \frac{1}{1-\lambda^2}\,. \tag{11}$$

Equation (11) can be solved numerically, and the corresponding curve is shown in figure 7(b). Note that, contrary to tokamaks [26], θ_b does not depend on radius. As expected, deeply trapped particles, namely particles with zero parallel velocity ($\lambda = 0$) have $\theta_b = \pi/2$, that is, they barely oscillate remaining on the equatorial plane. Bananas become more and more elongated when approaching the trapped-passing boundary, until they touch the origin at $\theta_b = 0$ for $\lambda = \lambda_c$. Note also that for the point dipole $\lambda_c = 1$, meaning that almost 100% of particles are trapped: only particles with velocity aligned with the field $\vec{B}$ are passing. This behavior is linked to the divergence of B for $r = 0$ in equation (7). In a real device there is no divergence, yet 90% of particles are trapped, as shown in figure 7(a).

A consequence of this preliminary analysis is that, due to the combination of banana motion and precession, *all trapped particles cross the equatorial plane at* $\theta = \pi/2$. This is an issue for the present design of the device, which shows three horizontal supports between the cylinder coil and the 'stew-pot' coils, see again figure 2(a). Even slanting the supports, e.g. at $\theta = 60°$ does not help much, since ∼20% of particles will eventually hit the supports, with a mechanism similar to Earth's auroras (see figure 7(b)). For this reason, a modified design with three current-carrying supports attached to a central stem at $z = 0$ is under consideration: also LDX had supports in the central hole of the superconducting ring, see figure 1 in [17]. This geometry minimizes particle losses because only passing particles hit the supports, and, according to figure 7(a), they are only 10% of all particles.

An example of a banana (trapped) and of a passing orbit in the device is shown in figure 8. The initial pitch of the particles are $\lambda = 0.58$ and $\lambda = 0.99$, respectively, which is consistent with the values of the critical pitch shown in figure 7(a). The particle trajectories are calculated by integration of the Newton-Lorentz equation of motion with a Boris algorithm [27], which—in absence of an electric field—automatically satisfies the conservation of energy $E = 1/2\, mv^2$. The error on magnetic moment $\mu = 1/2\, mv_\perp^2/B$ is also globally bounded [28]. A single electron is deposited at $Z = 0$ and $R = 7$ cm with an energy of $E = 10$ eV. For the electron energy, we use the value measured in the center of the magnetron dipole device [16]; the deposition radius has been chosen, in similarity with LDX, near the zero of the diamagnetic current, where β is predicted to be maximum [17]. From the trapped trajectory we can estimate the electron bounce time to be $\tau_b \sim 0.3\,\mu$s and the precession frequency $\omega_d \sim 1.6 \times 10^5\,\mathrm{rad\,s^{-1}}$ (corresponding to a real frequency $f_d \sim 25$ kHz). As a comparison, the same numbers for a trapped electron (pitch $\lambda = 0.4$) with energy $E = 800$ eV deposited at the reversal (where $B_\phi = 0$) for a typical reversed-field pinch discharge are $\tau_b = 1\,\mu$s and $\omega_d \sim= 1.3 \times 10^3\,\mathrm{rad\,s^{-1}}$ (real frequency $f_d \sim 210$ Hz). The precession frequency is two orders of magnitude larger than at the null surface $B_\phi = 0$ of a toroidal fusion device, due to the steep field gradient $\dfrac{\partial B}{\partial \Psi}$ which is the main characteristic of a dipole. Also the passing electron experiences a precession motion (this is a peculiarity of a dipole, as explained above), with a precession frequency of nearly the same order of magnitude, $\omega_d = 6 \times 10^4\,\mathrm{rad\,s^{-1}}$ (real frequency $f_d = 9.6$ kHz). To study more in detail and with higher precision particle trajectories in the phase space, the development of a more sophisticated Hamiltonian, guiding center code in spherical coordinates, using the analytic expression of the dipole field given in equation (6), is underway.

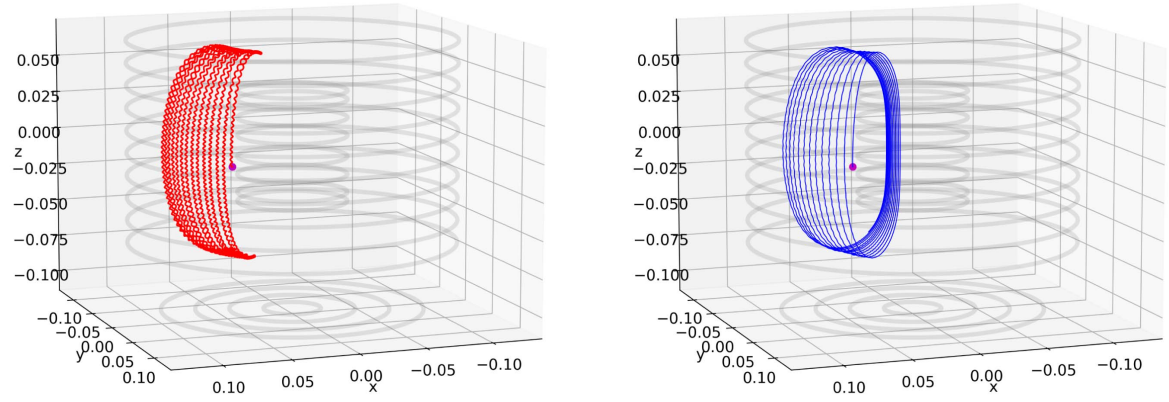

Figure 8. (a) Trapped (initial $\lambda = 0.59$) and (b) passing (initial $\lambda = 0.99$) electron trajectories in the device. The coil system is shaded in gray.

Finally, we can provide a rough estimate of the power consumption of our device by calculating a standard, 0D particle balance in Hydrogen, following [29]. We assume a power input $P_{abs} \approx 21$ kW and an equivalent loss area of $\approx 0.02\,m^{-2}$ (corresponding to the region of open field lines in figure 5(a)). We also make the conservative hypothesis of equal atomic and molecular Hydrogen densities, $n_H = n_{H_2}$ in the evaluation of the collisional energy loss $\mathcal{E}_c$ [30], and of a flat electron temperature radial profile with $T_e = 10$ eV. We obtain an electron density of the order $1 \times 10^{18}\,m^{-3}$, which is similar to the density obtained in present-day sources (1.5×10^{18} in SPIDER [31, 32]), but using a larger power, ∼50 kW per driver. The absorbed power $P_{abs} \approx 21$ kW proposed for the dipole device, is a reasonable number, since cold plasmas in this range of density and temperature ($n_e = 1 \times 10^{18}\,m^{-3}$ and $T_e = 10$ eV) are typically obtained in industrial applications with a power input $P_{abs} \lesssim 10$ kW [33]. The density obtained with the 0D balance is also consistent with the plasma beta $2\% \leqslant \beta \leqslant 19\%$ evaluated in section 2.1, which corresponds to a density in the interval $7 \times 10^{17} \leqslant n_e \leqslant 7 \times 10^{18}\,m^{-3}$. It is worth noting that the same density can be obtained with even lower P_{abs} if one relaxes the hypothesis of a flat electron temperature profile (which is expected in the dipole, due to the presence of the strong, transverse magnetic field).

4. Conclusions

In this paper we propose a novel prototype of negative ion source in Neutral Beam Injectors (NBI) for nuclear fusion applications. The prototype is based on a simple magnetic dipole configuration, with an axially symmetric magnetic field. The field is purely poloidal, with maximum amplitude ∼80 mT. We demonstrate that the device satisfies basic MHD equilibrium, with a purely toroidal diamagnetic current of ∼80 A, corresponding to ∼ 1% of the current flowing in the central coil. Plasma will be produced with a filament, or by RF and/or microwave heating (maximum frequency ∼2 MHz and 2 GHz, respectively). We estimate that the plasma will possess a beta parameter in the range $\beta \approx 2 - 19\%$: if it is feasible experimentally to reach the upper bound 19%, this will imply a much higher plasma current of ∼890 A. Particles follow closed orbits on the poloidal plane, with negligible drifts across the flux surfaces since $B_\phi = 0$, and precede with a velocity proportional to the radial derivative of the magnetic field. Almost all particles (∼ 90%) are trapped in the magnetic mirror, thus we expect that our device will possess a good particle confinement. In order to reduce the unavoidable interaction of energized plasma particles with the supports of the central cylinder coils, the current-carrying supports can either be magnetically shielded as proposed in [15], or positioned inside the central cylinder coil, where the plasma density is expected to be much lower than outside.

The proposed ion source is promising under many aspects: the dipole magnetic configuration is well-known in geophysics, it is a rather simple geometry to be realized in laboratory, it is characterized by an intrinsic high beta and good particle confinement, and, last but not least, the magnetic field is placed inside the ion source, which is a considerable advantage with respect to present-day source schemes since it reduces the input power to $P_{abs} \approx 20$ kW or less. In this respect, the main advantage of the dipole source over the existing ones is the expected reduction of the required input power for producing a plasma with the same parameters. In addition, the dipole magnetic configuration already includes the transverse magnetic field necessary for filtering out the $E \gtrsim 1$ eV electrons before they reach the negative ion production region.

We are now planning the construction of a small proof-of-concept device. For the first plasma experiments we will probably use a simple filament-driven arc discharge. We expect that one of the critical issues to be tackled in the design and during experiments will be related to the heat load on the

current-carrying supports (feeders) of the central cylinder coil. As mentioned in section 2 and shown in figure 2(a), these components necessarily intercept the plasma flux surfaces in a small area. For this reason, they will be water cooled and will be shaped so as to produce a local magnetic shield, which should deflect the charged particle trajectories and reduce the interaction with plasma. However, at the moment, no experimental data or reliable model is available for estimating the efficiency of this kind of local magnetic shield.

A second expected issue could be related to the magnitude of the plasma diamagnetic current, which we have estimated to be not smaller than 1% of the central cylinder coil current. However, this value is based on experiments on larger devices (such as LDX) and might be optimistic in a very small device.

Data availability statement

The data cannot be made publicly available upon publication because no suitable repository exists for hosting data in this field of study. The data that support the findings of this study are available upon reasonable request from the authors.

Acknowledgments

We wish to acknowledge the support of our colleagues Roberto Cavazzana, Emilio Martines and Matteo Zuin for the development of the project of the dipole experiment, and we thank Piergiorgio Sonato for interesting insights into the physics of ion sources. One of the Authors (G S) wishes to thank Roscoe B. White for fruitful discussions on particle motion in a dipole field.

ORCID iDs

G Chitarin https://orcid.org/0000-0003-3060-8466
D Abate https://orcid.org/0000-0002-0331-3454
G Spizzo https://orcid.org/0000-0001-8586-2168

References

[1] Toigo V *et al* 2017 *New J. Phys.* **19** 085004
[2] Kuriyama M *et al* 1998 *J. Nucl. Sci. Technol.* **35** 739–49
[3] Fantz U *et al* 2022 *J. Phys.: Conf. Ser.* **2244** 012049
[4] Zielke D, Briefi S and Fantz U 2021 *J. Phys. D: Appl. Phys.* **54** 155202
[5] Ichikawa M, Kojima A, Hiratsuka J, Yoshida M, Umeda N, Squilayan G Q, Watanabe K, Tobari H and Kashiwagi M 2020 *Rev. Sci. Instrum.* **91** 023502
[6] Wurzel S E and Hsu S C 2022 *Phys. Plasmas* **29** 062103
[7] Chitarin G, Abate D, Elio F, Sartori E and Spizzo G 2023 A novel plasma source concept for negative ion generation in neutral beam injectors for fusion applications *Proc. 20th Int. Conf. on Ion Sources - ICIS'23 (Victoria, BC, Canada)* (TRIUMF Canada's Particle Accelerator Centre) p 106
[8] Schulz M and Lanzerotti L J 1974 *Adiabatic Invariants and Magnetospheric Models* (Springer) pp 10–45
[9] Freidberg J P 2014 *Ideal MHD* 2nd edn (Cambridge University Press) ch 11.4.4, pp 452–8
[10] Hasegawa A 1987 *Comments Plasma Phys. Control. Fusion* **11** 147–51
[11] Garnier D T, Kesner J and Mauel M E 1999 *Phys. Plasmas* **6** 3431–4
[12] Garnier D, Boxer A, Ellsworth J, Kesner J and Mauel M 2009 *Nucl. Fusion* **49** 055023
[13] Elio F 2014 *Fusion Eng. Des.* **89** 806–11
[14] Lehnert B 1958 *Nature* **181** 331–2
[15] Lehnert B 1959 *J. Nucl. Energy* C **1** 40
[16] Martines E, Zuin M, Marcante M, Cavazzana R, Fassina A and Spolaore M 2016 *Phys. Plasmas* **23** 053511
[17] Garnier D T, Hansen A, Mauel M E, Ortiz E, Boxer A C, Ellsworth J, Karim I, Kesner J, Mahar S and Roach A 2006 *Phys. Plasmas* **13** 056111
[18] Freidberg J P 2014 *Ideal MHD* 2nd edn (Cambridge University Press) ch 6.4.3, p 140
[19] Karim I 2007 Equilibrium and stability studies of plasmas confined in a dipole magnetic field using magnetic measurements *PhD Thesis* Dept. of Nuclear Science and Engineering Massachusetts Institute of Technology (MIT) (available at: http://hdl.handle.net/1721.1/41294)
[20] Davis M S, Mauel M E, Garnier D T and Kesner J 2014 *Plasma Phys. Control. Fusion* **56** 095021
[21] Abate D and Bettini P 2019 *Plasma Phys. Control. Fusion* **61** 105016
[22] Davis M S 2013 Pressure profiles of plasmas confined in the field of a dipole magnet *PhD Thesis* Applied Physics and Applied Mathematics Columbia University (https://doi.org/10.7916/D84X5G08)
[23] Jackson J D 1998 *Classical Electrodynamics* 3rd edn (Wiley) ch 5.6, p 186
[24] White R B 2014 *The Theory of Toroidally Confined Plasmas* 3rd edn (Imperial College Press) pp 79–80
[25] Gobbin M, Guazzotto L, Guo S C, Predebon I, Sattin F, Spizzo G, Zanca P and Cappello S 2009 Trapped particles in the reversed field pinch *J. Plasma Fusion Res.* **8** 1147–52 (available at: www.jspf.or.jp/JPFRS/PDF/Vol8/jpfrs2009_08-1147.pdf)
[26] White R B 2014 *The Theory of Toroidally Confined Plasmas* 3rd edn (Imperial College Press) pp 96–97
[27] Boris J 1970 *Proc. 4th Conf. on Numerical Simulation of Plasmas* (Naval Research Laboratory) p 3
[28] Qin H, Zhang S, Xiao J, Liu J, Sun Y and Tang W M 2013 *Phys. Plasmas* **20** 084503
[29] Lieberman M A and Lichtenberg A J 2005 *Particle and Energy Balance in Discharges* (Wiley) ch 10, pp 327–86
[30] Samuell C M and Corr C S 2015 *Plasma Sources Sci. Technol.* **25** 015014
[31] Sartori E *et al* 2021 *Fusion Eng. Des.* **169** 112424
[32] Jain P, Recchia M, Sartori E, Serianni G, Poggi C, Ugoletti M and Zaniol B 2023 *Plasma Phys. Control. Fusion* **65** 095010
[33] Chen F F 2007 *Radiofrequency Plasma Sources for Semiconductor Processing* (Wiley) ch 6, p 114